Fractal Structure of 2D Mueller Matrix Images of Biotissues

O.V.Angelsky, A.G.Ushenko*, Yu.A.Ushenko, A.O.Angelskaya

Chernivtsi National University, 2 Kotsyubinsky St., 58012 Chernivtsi, Ukraine,
*ushenko-bio@itf.cv.ukrtel.net

Received: 30.10.2004

Abstract

Interconnections between a geometric structure of biotissues and their polarization properties have been studied. It has been shown that a fractal character of those properties for physiologically normal biotissue transforms into multifractal for pathologically changed one.

Keywords: Mueller matrix, biotissue, tomography, fibril, polarization

PACS: 42.62.-b, 42.62.Be, 42.25.Lc, 42.25.Ja, 81.70.Tx

1. Introduction

Measuring Stokes vector of a light scattered by biotissues (BT) and calculating a corresponding Mueller matrix enables one to obtain the most complete (statistically averaged over the whole set of bioobject's inhomogeneities) information on their polarization properties [1]. The analysis of such the information looks promising for the studies of macrostructure of various BT in frame of the problems related to biomedical diagnostics of their physiological state. Techniques for a non-destructive optical coherent tomography (OCT) [2, 3], as well as its novel branch, a polarization-sensitive OCT (PSOCT) [4-8], which is based on measuring depth-resolved, 2D spatial distribution of the Mueller matrix components (or Mueller-matrix images, MMI) with high space resolution (~ 1μm) and high scanning speed [9-12], represent a very important direction of the diagnostics.

The MMI analysis allows obtaining a vital biomedical information on both the geometric macrostructure of the BT and the value and coordinate distributions of optical parameters related to anisotropy of their architectonic nets made up by geometrically self-similar bundles of collagen myosin, etc. [13-14]. Further progress in the PSOCT should be associated with elaborating new methods for the MMI analysis and a further search for diagnostically urgent interconnections of their structure with the geometric parameters of the architectonics, determining physiological state of the BT.

This paper presents the results of studying interconnections between the self-similar geometry of the BT structure and the peculiarities of manifestation of their polarization properties, which are quite completely described by the set of 2D Mueller matrix components.

The investigation is based on the following principles:

1. Geometry of the BT architectonics reveals a hierarchical, self-similar thread-like structure (microfibrils, fibrils, fasciae, fibres and bundles as "structural elements"). The structural elements are discrete and they are characterized with a scaling recurrence in a wide range of optical scales (1–1000 μm). "Flat" and 3D spatial twist-effects occurring in transformation of the orientations and dimensions of fibrillar components – an analogue of the affine

transformations that form mathematical fractals [14] – are growth mechanisms for the architectonic nets. It would be therefore appropriate to assume a fractal nature of its geometric structure, defined by self-similar coordinate ((X,Y)) distributions of both the scales of the structural elements (here we distinguish between the corresponding transverse and the longitudinal ($d(X,Y)$) measures) and their orientations (i.e., the angular directions $\rho(X,Y)$ of the fibril packing with respect to the plane of the BT layer under analysis).

2. As optical objects, the structural elements of the BT architectonics hierarchy manifest the properties of optically uniaxial crystals, the optical axis direction of which is determined by the $\rho(X,Y)$ parameter, while the birefringence value Δn is related to the properties of fibril substance [15]. Scaling self-similarity of their geometric sizes enables one to assume analogous self-similar nature for the phase shift ($\delta(X,Y)=\left(2\pi/\lambda\right)\Delta n d(X,Y)$) between orthogonally polarized light wave components (the wavelength λ) passing through the BT.

3. The BT can be morphologically presented by a two-component (amorphous-crystalline) structure [15]. That is why, the Mueller matrix of the BT layer analysed with the PSOCT is determined by superposition of the partial operators of its amorphous ($\{a_{ik}\}$) and ($\{c_{ik}\}$) crystalline components:

$$\{B\}=\begin{Vmatrix} 1 & 0 & 0 & 0 \\ 0 & c_{22}+a_{22} & c_{23} & c_{24} \\ 0 & c_{32} & c_{33}+a_{33} & c_{34} \\ 0 & c_{42} & c_{43} & c_{44}+a_{44} \end{Vmatrix}, \quad (1),$$

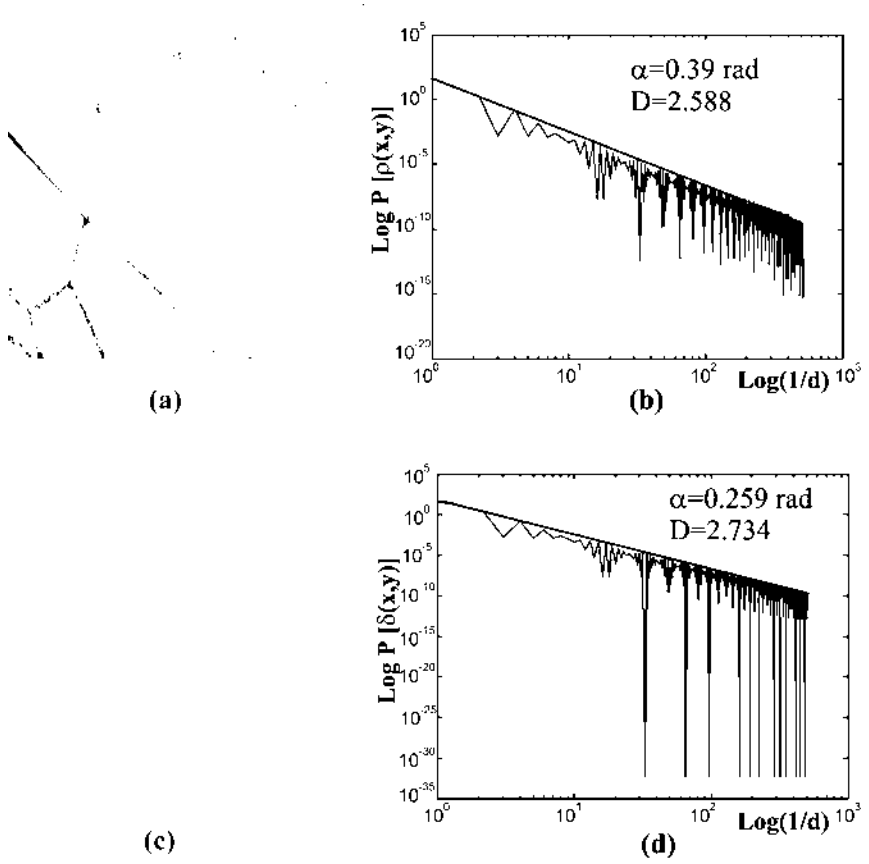

Fig. 1. Log-log dependences of the power spectra for model fractal distributions of (b) the orientation parameter $\rho(X,Y)$ (corresponding to the butterfly's wing image, a) and (d) the phase parameter $\delta(X,Y)$ (corresponding to the bone tissue image, c), obtained for the case of crossed polarizers.

$$
\begin{aligned}
&a_{22} \approx a_{33} \approx a_{44} = e^{-\tau L} \\
&c_{22} = \cos^2 2\rho + \sin^2 2\rho \cos\delta, \\
&c_{23} = c_{32} = \cos 2\rho \sin 2\rho (1 - \cos\delta), \\
&c_{24} = -c_{42} = -\sin 2\rho \sin\delta, \\
&c_{33} = \sin^2 2\rho + \cos^2 2\rho \cos\delta, \\
&c_{34} = -c_{43} = \cos 2\rho \sin\delta, \\
&c_{44} = \cos\delta
\end{aligned}
\qquad (2).
$$

Here τ is the optical extinction coefficient of the BT layer with the thickness L.

It follows from Eqs. (1) and (2) that the geometric (i.e., orientation $\rho(X,Y)$) and the optical (or phase-shifting $\delta(X,Y)$) parameters of structural elements in the architectonic nets play a deciding role in transformations of the polarization state. The impact of these two factors on the MMI set $c_{ik}(X,Y)$ may be regarded as a result of multiplication of several coordinate-dependent fractal multivariable functions $F_{mn}[\rho(X,Y);\delta(X,Y)]$ [16].

Fig. 1 and 2 represent the results of modelling studies for the fractal structure of the MMI $c_{ik}(X,Y)$ formed by superposition of 2D sets of the parameters $\rho(X,Y),\delta(X,Y)$, possessing an *a priori* monofractal structure. The following objects have been used as the models:

- The microscopic image of a butterfly's wing (see Fig. 1a) as an analogue of 2D $\rho(X,Y)$ set;
- The plate of the cannon-bone tissue with the geometric thickness of 25 μm (its image $I_\delta(X,Y)$ in the crossed quarter-wavelength plates is presented in Fig. 1c) as an analogue of 2D set of the phase shifts $\delta(X,Y) = \sqrt{\arcsin[I_\delta(X,Y)]}$.

The fractal dimension of the intensity distributions $I(X,Y)$ for the images of both types has been calculated with the technique described in [17], i.e.

- the 2D correlation functions $K_{X,Y}[I(X,Y)]$ have been determined;
- log-log dependences of the power spectra for the autocorrelation functions of MMI

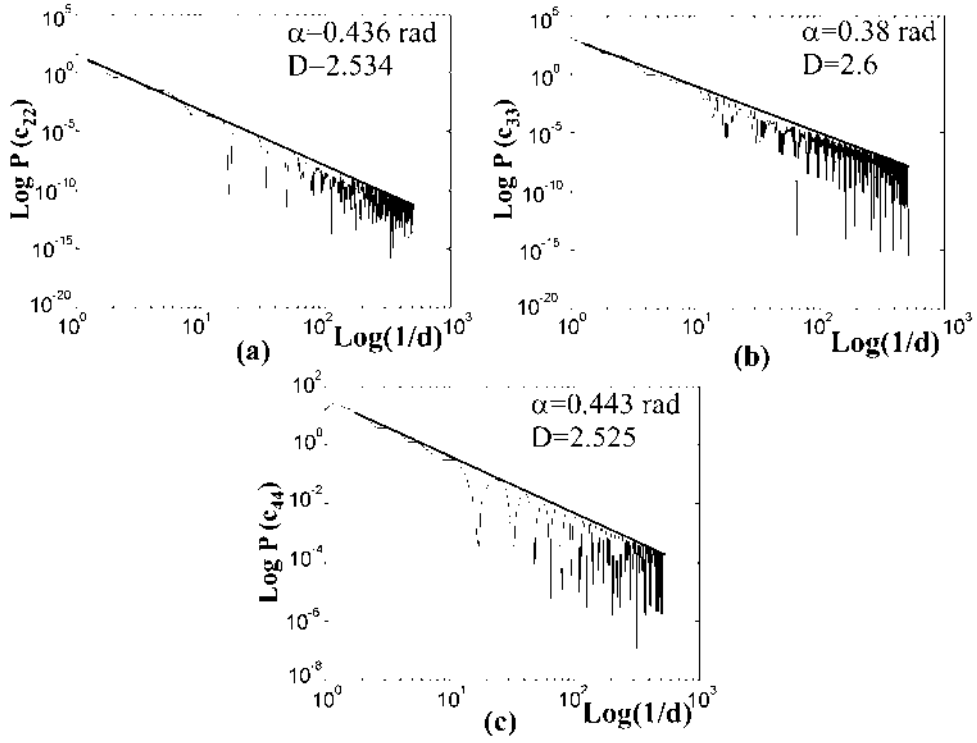

Fig. 2. Log-log dependences of the MMI power spectra for a model architectonic net with fractal structure of both the orientation $\rho(X,Y)$ and the phase $\delta(X,Y)$.

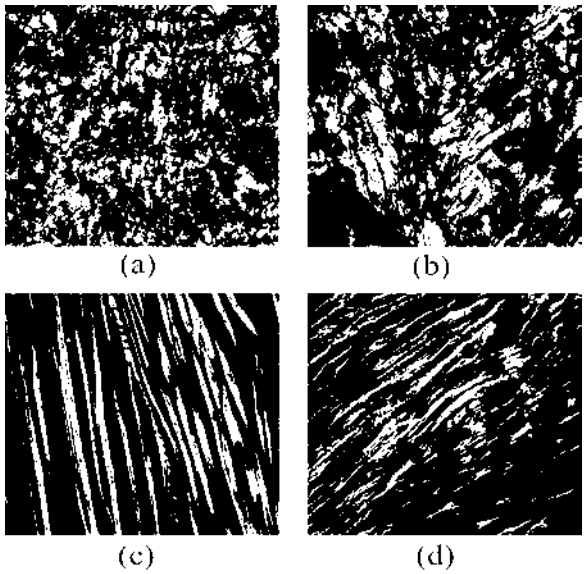

Fig. 3. Polarization images of architectonic nets in the histological SD (a, b) and MT (c, d) sections, obtained for the case of crossed polarizers. Parts (a) and (c) illustrate the architectonic structure of physiologically normal samples and (b) and (d) that of pathologically and degeneratively-dystrophically changed samples.

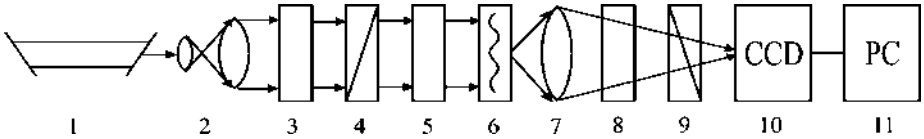

Fig. 4. Experimental setup: 1, He-Ne laser; 2, collimator; 3, 5 and 8, quarter wave plates; 4, polarizer; 9 analyser; 6, object under test; 7, microobjective; 10, CCD camera; 11, personal computer.

($\mathrm{P}_j\left\{\log \mathrm{K}_{X,Y}\left[I(X,Y)\right];\log\left[d^{-1}(X,Y)\right]\right\}$) and the slopes of their envelopes ($\left\{\alpha_j\left[I(X,Y)\right]\right\}$) have been found, according to which the fractal dimensions $\left\{D^{(j)}\left[I(X,Y)\right]\right\}$ of $I(X,Y)$ have been calculated using the relation

$$D^{(j)}\left[I(X,Y)\right] = 3 - \tan\left\{\alpha_j\left[I(X,Y)\right]\right\}. \qquad (3)$$

It is seen from the data obtained that the 2D intensity distributions for the microscopic ($I(X,Y)$) and polarization-filtered ($I_\delta(X,Y)$) images possess a monofractal nature in case of the samples of both types. Namely, the coordinate distribution of the fibres' packing orientations $\rho(X,Y)$ has the dimension $\left\{D^{(j)}\left[I(X,Y)\right]\right\}$ = 2.588 for the butterfly's wing architectonic net (Fig. 1b), where the coordinate distribution of the phase shift $\delta(X,Y)$ produced by the substance of mineralised bone-tissue (Fig. 1d) has the dimension $\left\{D^{(j)}\left[I(X,Y)\right]\right\}$ = 2.734.

Fig. 2 shows a series of model dependences $\mathrm{P}_j\left\{\log \mathrm{K}_{X,Y}\left[c_{ik}(X,Y)\right];\log\left[d^{-1}(X,Y)\right]\right\}$ obtained for the set of 2D distributions of the matrix elements $c_{ik}(X,Y) = f_{ik}\left[\rho(X,Y),\delta(X,Y)\right]$ in case of the object possessing a fractal architectonic structure in both the orientations of its elements (see Fig. 1b) and in the phase-shifting ability of the substance (see Fig. 1d). One can see that (i) the set of the MMI elements $c_{ik}(X,Y)$ for the object with fractal geometric architectonic structure is fractal, too (Fig. 2a–c), and (ii) the fractal dimensions $\left\{D^{(j)}\left[c_{ik}(X,Y)\right]\right\}$ of the MMI elements $c_{ik}(X,Y)$, possessing different functional structure, are different. Thus, the fractality of the structure of certain

geometric and optically anisotropic components of the object's architectonics manifests itself at the level of its polarization properties, which are completely described by the set of elements $c_{ik}(X,Y)$ of the corresponding Mueller matrix.

2. Characteristics of investigation objects

Optically thin ($\tau \le 0.1$ cm^{-1}, see also the thickness values) histological sections of normal and pathologically changed (due to psoriasis and muscular dystrophy) human skin derma (SD) and muscular tissue (MT) have been investigated. They possess the following geometric and optical parameters (see [18, 19]):

- SD: the absorption coefficient μ_a = 2.2 cm^{-1}, the scattering coefficient μ_s = 185 cm^{-1}, the anisotropy parameter g = 0.82 and the geometric thickness L = 30 μm;
- MT: μ_a = 2 cm^{-1}, μ_s = 215 cm^{-1}, g = 0.96 and L = 30 μm.

The objects under test have been chosen with the following motives:

- the optical parameters of these BT are similar, i.e. the architectonic nets are formed by the protein (both collagen and myosin) bundles

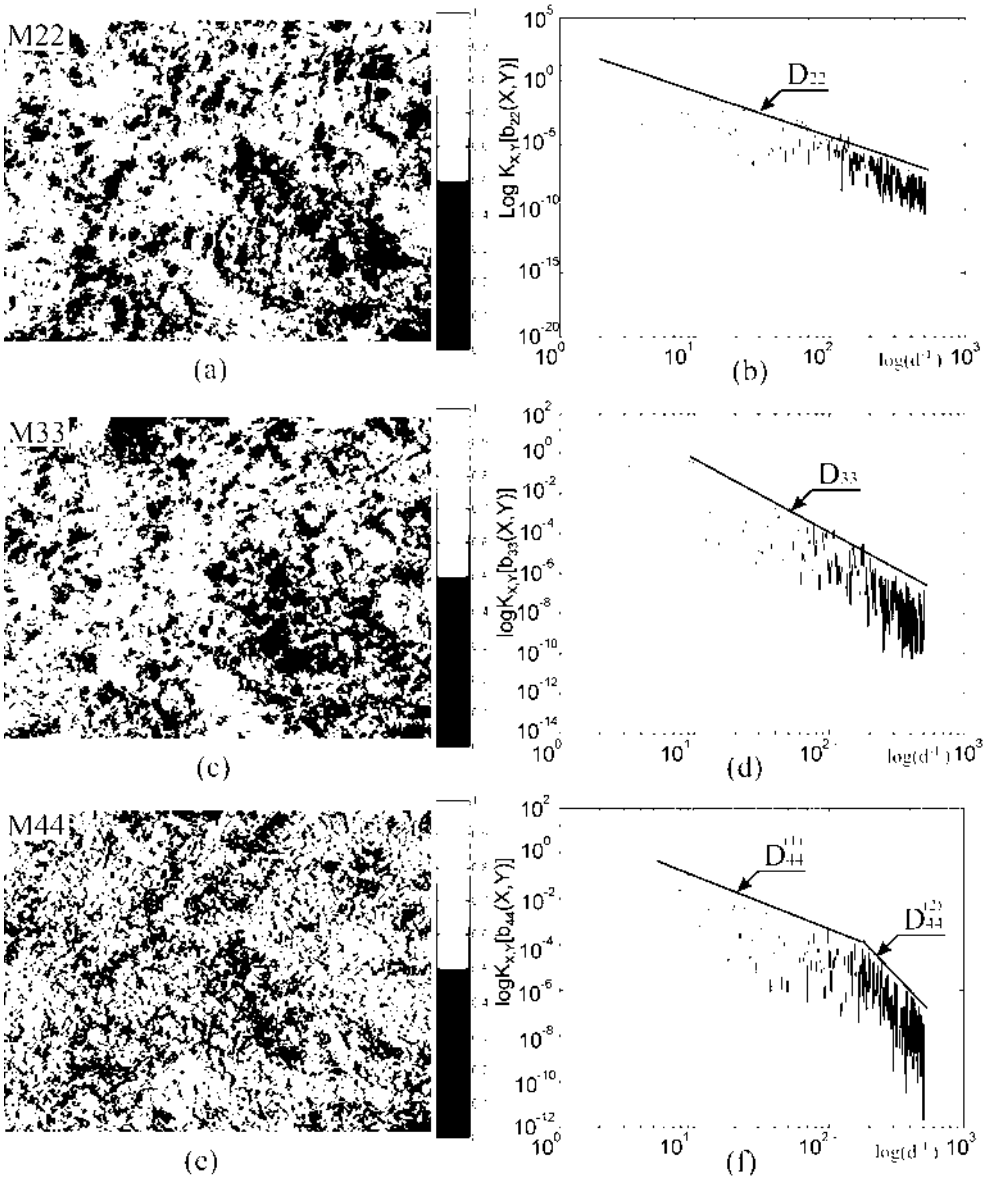

Fig. 5. Coordinate structures (a, c and e) and log-log dependences of the power spectra (b, d and f) for the MMI elements of physiologically normal SD.

(see Fig. 3d), with the similar birefringence values ($\Delta n(DS) \approx \Delta n(MT) = 1.5 \times 10^{-3}$);

- the geometric parameters are different as much as possible, i.e. the architectonic net of the MT is rather ordered, according to the direction of fibres packing, while, on the contrary, the SD is disordered (see Fig. 3a and c);
- the pathological changes are morphologically accompanied by formation of the "growth directions" and increase in the sizes of collagen fibres (Fig. 3a and c), while the myosin fibres of the MT are disordered and become thinner (Fig. 3b and d).

3. Optical scheme

Fig. 4 shows the optical scheme for measuring the BT MMI . The BT was illuminated by a collimated He-Ne laser beam (∅ = 10^4μm, λ = 0.6328 μm). Polarization illuminator (quarter-wavelength plates 3 and 5 and a polarizer 4) formed a set of Stokes vectors of the illuminating beam $\left\{S^{IL}_{j=1,2,3,4}\right\}$. By means of microobjective 7, polarized images of the BT were projected onto the plane light-sensitive area (800x600 pixels in square) of a CCD camera, which provided the measuring range 2–2000 μm for the structural elements of BT.

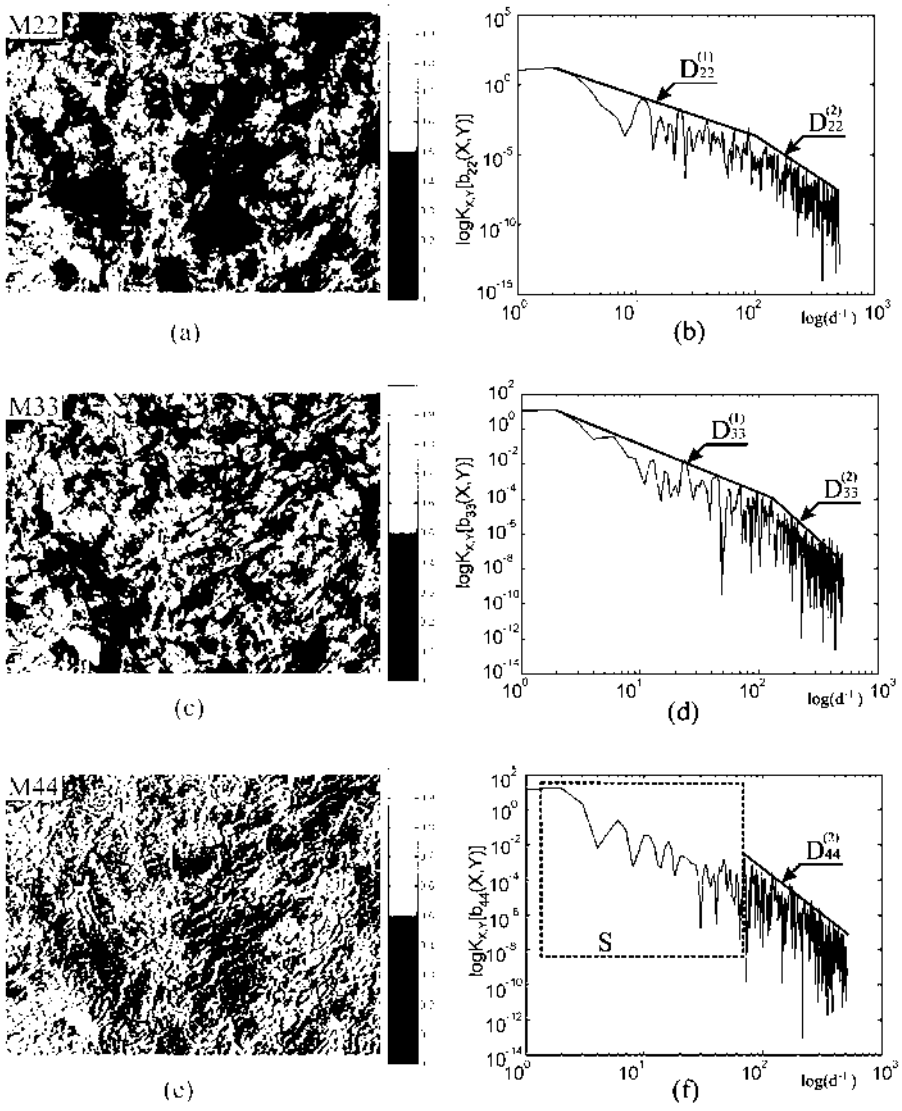

Fig. 6. Coordinate structure (a, c and e) and log-log dependences of the power spectra (b, d and f) for the MMI elements of pathologically changed SD. S mean the areas of statistical distribution.

The conditions of the experiment were chosen so as to enable reducing the space-angular aperture filtering, while forming the BT images. This was ensured by matching the angular characteristics of light scattering indicatrices of the BT samples ($\Omega \approx 16^0$, with Ω being the plane angle of the cone, in which 98% of all the light-scattered radiation energy is concentrated) and the angular aperture of the microobjective ($\Delta\omega = 20^0$).

The BT images were analysed with the system consisted of a quarter-wavelength plate 8 and a polarizer 9. As a result, the Stokes vectors of the BT images ($\left\{S^{BT}_{j=1,2,3,4}\right\}$) were determined and the MMI set $c_{ik}(X,Y)$ was calculated according to the algorithm

$$\begin{aligned} c_{i1} &= 0.5\left[S_i^{(1)} + S_i^{(2)}\right], \\ c_{i2} &= 0.5\left[S_i^{(1)} - S_i^{(2)}\right], \\ c_{i3} &= S_i^{(3)} - c_{i1}, \\ c_{i4} &= S_i^{(4)} - c_{i1}\ (i = 1,2,3,4). \end{aligned} \tag{4}$$

Here the indices "1" to "4" correspond to the following polarization states of the illuminating beam: 1 – 0^0, 2 – 90^0, 3 – $+45^0$ and 4 – $\otimes$ (a right-handed circular polarization).

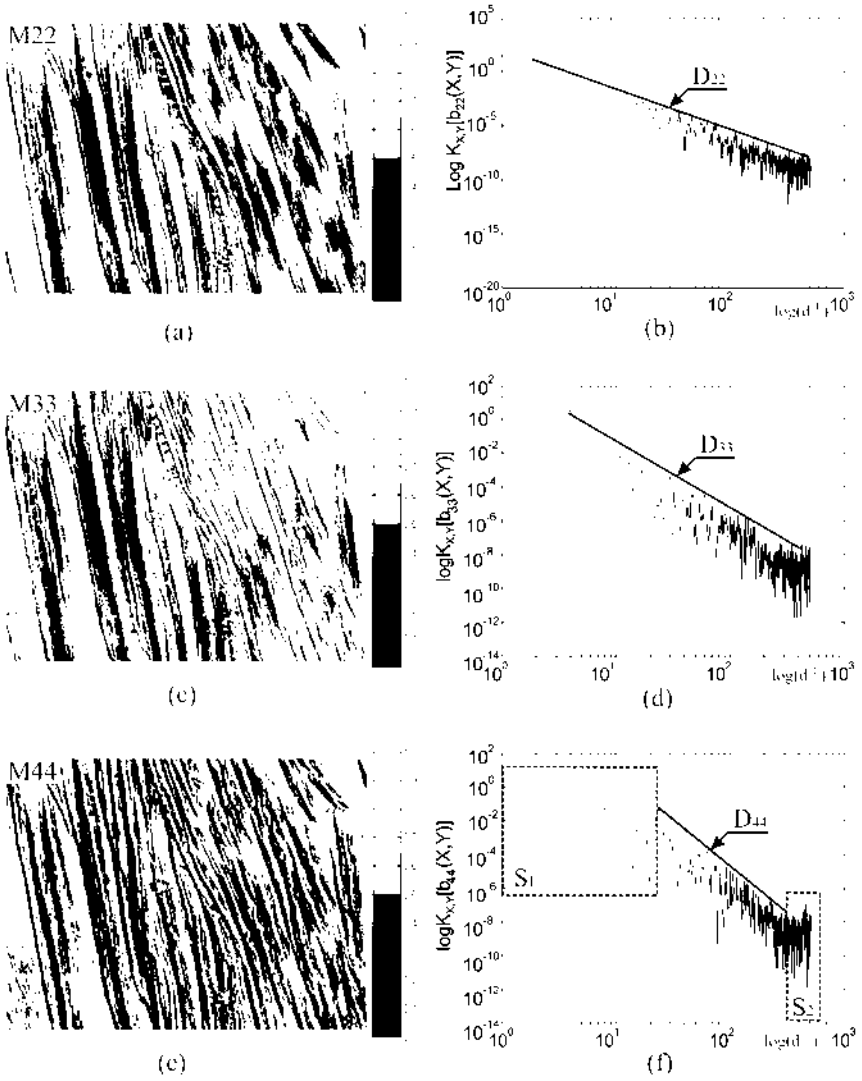

Fig. 7. Coordinate structure (a, c and e) and log-log dependences of the power spectra (b, d and f) for the MMI elements of physiologically normal MT. S mean the areas of statistical distribution.

4. Analysis and discussion of experimental data

The results for the structure of coordinate distributions of the MMI set for all the BT types are presented in Fig. 5 to 8. In particular, Fig. 5 and Fig. 6 show $c_{ik}(X,Y)$ (left column) and the corresponding $\mathrm{P}_j\left\{\log \mathrm{K}_{X,Y}\left[c_{ik}(X,Y)\right];\log\left[d^{-1}(X,Y)\right]\right\}$ calculated for physiologically normal (Fig. 5) and pathologically changed (Fig. 6) SD samples. Fig. 7 and Fig. 8 illustrate the same results for the polarization properties of MT samples.

The data obtained testify the following:

- the MMI $c_{22,33}(X,Y)$ for physiologically normal BT of both types are characterized by practically monofractal structure ($\left\{D^{(j)}\left[c_{ik}(X,Y)\right]\right\} \approx$ const) in the range of structural architectonic elements as large as almost three orders of magnitude (2–10^3 μm, see Fig. 5b, d and Fig. 7b, d);
- the fractal dimensions of MMI $c_{22,33}(X,Y)$ for different matrix components do not coincide with each other (we have $D_{22}=2.63$ and $D_{33}=2.46$ for the SD and $D_{22}=2.45$ and $D_{33}=2.36$ for the MT);
- the coordinate structure of the MMI element $c_{44}(X,Y)$ is multifractal for physiologically normal SD ($D_{44}^{(2)}(2\div 8\mu m)=2.18$ and $D_{22}^{(1)}(8\div 800\mu m)=2.58$ – see Fig. 5f).
- the fractal structure of the MMI element $c_{44}(X,Y)$ for physiologically normal MT is observed for the medium scales of myosin fibres in the architectonic net ($D_{44}(5\div 90\mu m)=2.38$ – see Fig.7f);
- the processes of pathological changes in the SD structure are accompanied with the changes in their geometric and optical properties (see Fig. 3b), namely, the fractal MMI structure for the elements $c_{22,33}(X,Y)$ is transformed into multifractal one (Fig. 6a and c). Furthermore, new additional fractal dimensions appear ($D_{22}^{(2)}(2\div 10\mu m)=2.38$, $D_{22}^{(1)}(10\div 800\mu m)=2.71$ – see Fig. 6b, and $D_{33}^{(2)}(2\div 10\mu m)=2.09$, $D_{33}^{(1)}(10\div 800\mu m)=2.58$ – Fig. 6d). The MMI element $c_{44}(X,Y)$ keeps its fractal structure within only small collagen fibril sizes ($D_{44}(2\div 20\mu m)=2.11$ – see Fig. 6f). For the larger scales of architectonic net elements, the coordinate distribution for $c_{44}(X,Y)$ is transformed into a statistic one;
- degenerative-dystrophic changes in the MT become evident in the appearance of new dimensions ($D_{22}^{(2)}(2\div 20\mu m)=2.18$, $D_{22}^{(1)}(50\div 800\mu m)=2.45$ – see Fig. 7b) and "destruction" of fractal structure of the MMI elements $c_{22,33}(X,Y)$ for the large and medium scales of myosin fibres and their architectonics ($D_{22}\neq const\ (20\div 50\mu m)$, $D_{33}\neq const\ (20\div 800\mu m)$ and $D_{44}\neq const\ (8\div 800\mu m)$ – see, respectively, Fig. 7b, d and f). In other words, then the values $\left\{\alpha_j\left[c_{ik}(X,Y)\right]\right\}$ change chaotically.

Table 1 presents the ranges of change in the fractal dimensions $D_{ik}^{(j)}$ for the MMI elements $c_{ik}(X,Y)$, determined using a set of 37 physiologically normal and 41 pathologically changed SD samples. Besides, Table 2 illustrates the same values, determined using a set of 32 physiologically normal and 31 degeneratively-dystrophically changed MT samples.

Let us now analyse the above data in a more detail. The whole set of Mueller matrix components of the investigated BT characterizes different transformation mechanisms for the optical polarization state. Moreover, a decisive contribution into this process is made by optically anisotropic BT component, whose polarization properties are described with the set

of $c_{ik}(X,Y)$ elements. One can pick out two main groups among them. The first group represents the "orientation" elements, connected with different directions of packing $\rho(X,Y)$ of the architectonic nets' fibrils. The MMI $c_{22}(X,Y) \to \begin{cases} \rho(X,Y) \equiv 0^0 \leftrightarrow 90^0 \\ \delta(X,Y) \equiv \cos\delta \end{cases}$ and $c_{33}(X,Y) \to \begin{cases} \rho(X,Y) \equiv +45^0 \leftrightarrow -45^0 \\ \delta(X,Y) \equiv \cos\delta \end{cases}$ belong to that group. They characterize the influence on transformation of polarization state by the fibrils (for the all "optical" scales of their hierarchy) for different orientations $\rho(X,Y)$, under the conditions of invariable "phase factor" $\delta(X,Y)$. The second group is the "phase" mechanisms, associated with anisotropy of the substance of optically uniaxial fibrils ($\delta(X,Y)$). They are characterized the best way with the MMI element $c_{44}(X,Y) \to \begin{cases} 0^0 \le \rho(X,Y) \le 180^0 \\ = \cos\delta(X,Y) \end{cases}$ that describes phase-shifting ability of the architectonics substance of the BT *per se*. Finally, specific features of the parameter distribution, characterizing both the optical ($\delta(X,Y)$) and geometric ($\rho(X,Y)$) structures of the BT architectonics samples, results in various fractal dimensions of the MMI elements $c_{ik}(X,Y)$.

On the other hand, pathological processes manifest themselves in formation of new growth directions, increase in the fibrils' scales and the concentration of optically anisotropic proteins [14]. Similar geometric and optical changes in the BT architectonics lead to appearance of newly formed nets, which are characterized by completely or partially different geometric self-similarity of fibril structures, including the orientation $\{\{\rho^*(X,Y)\}\}$ and the scale $\{\{d^*(X,Y)\}\}$ ones. Pathological changes in the orientation characteristics of architectonics of SD samples under study reveal themselves optically in appearing new slopes $\{\alpha_j[c_{ik}(X,Y)]\}$ for the envelopes of the power spectra $\mathrm{P}_j\{\log \mathrm{K}_{X,Y}[c_{ik}(X,Y)]; \log[d^{-1}(X,Y)]\}$. This occurs for the set of 2D distributions of the "orientation" elements $c_{22,33}(X,Y)$ for pathologically changed BT (cf. the data of Fig. 6 with those peculiar for physiologically normal BT – see Fig. 5). The coordinate MMI structure for those elements is transformed into multifractal one in case of the SD changed by

Table 1. Change ranges for the fractal dimensions of physiologically normal (37 samples) and pathologically changed (41 samples) SD.

c_{ik} components	D_{ik} (normal)		D_{ik} (changed)	
c_{22}	2.55 – 2.73		2.55 – 2.73	2.25 – 2.40
c_{33}	2.45 - 2.60		2.45 - 2.60	2.05 – 2.20
c_{44}	2.50 – 2.60	2.15 – 2.30	-	2.15 – 2.30

Table 2. Change ranges for the fractal dimensions of physiologically normal (32 samples) and pathologically changed (31 samples) MT.

c_{ik}	D_{ik} (normal)	D_{ik} (changed)	
c_{22}	2.40 – 2.60	2.40 – 2.60	2.15 – 2.25
c_{33}	2.30 - 2.45	-	2.10 – 2.15
c_{44}	2.35 – 2.45	-	2.05 – 2.15

psoriasis.

Self-similarity of MMI for the "phase" elements $c_{44}(X,Y)$ of the SD samples changed by psoriasis is kept only within very small scales of structural architectonic elements (2–20 μm). "Destruction" of the fractal structure of coordinate distributions for the phase shifts $\delta(X,Y)$ within the limits of large ranges of fibril scales may be prescribed to chaotic increase in the concentration of optically anisotropic proteins. Optically, it would manifest itself in a statistic character of changes for the parameter $c_{44}(X,Y)$.

Morphologically, disorientation and decrease in geometric scales of fibres and degradation of their optical anisotropy accompany the processes of degenerative-dystrophic changes of the BT architectonics on the early stage of appearance of the latter changes [14]. For the investigated samples of MT, these geometric changes of the structure break, first of all, the macroscale (10–800 μm) self-similar structure of the architectonic net. Optically this process becomes clear after statistical processing of coordinate distributions for the MMI elements $c_{22,33}(X,Y)$. There is practically no "stable" slope $\{\alpha_j[c_{ik}(X,Y)]\}$ of the power spectra

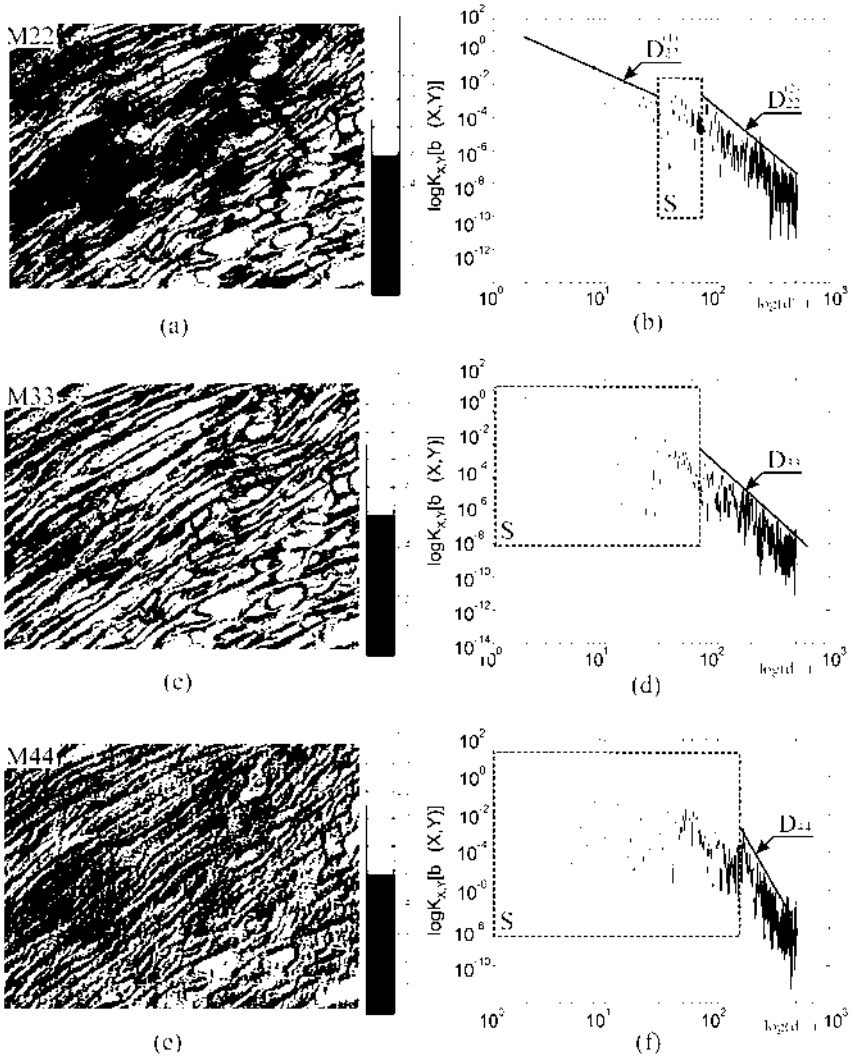

Fig. 8. Coordinate structure (a, c and e) and log-log dependences of the power spectra (b, d and f) for the MMI elements of degeneratively-dystrophically changed MT. S mean the areas of statistical distribution.

$P_j\left\{\log K_{X,Y}\left[c_{ik}(X,Y)\right];\log\left[d^{-1}(X,Y)\right]\right\}$ in the mentioned scale range (see Fig. 8b and d). At the same time, the optical properties determined by geometry of small-scale fibrils (2–10 μm) in the MT samples keep their fractal character (see Fig. 8b, d and f).

Self-similarity of the MMI for the "phase" elements $c_{44}(X,Y)$ is not observed in practice for dystrophically changed MT samples (see Fig. 8f). This may be related to chaotic decrease in the optical birefringence value for the myosin fibrils, determining the coordinate distribution of the phase shift $\delta(X,Y)$.

Conclusions

It has been demonstrated that the fractal geometric structure of the architectonic nets of physiologically normal BT of various morphologies manifests itself in the fractal character of their polarization properties described by a set of 2D elements of the Mueller matrices. The processes of pathological changes in the BT architectonics reveal themselves in appearing new fractal dimensions, together with forming a multifractal structure of the MMI for the "orientation" elements and destructing a large-scale fractal structure of the MMI for the "phase" elements. Degenerative-dystrophic changes are accompanied with randomisation of coordinate distributions of the Mueller matrices for the "orientation" elements of large-scale architectonic elements and a complete destruction of fractal structure for the MMI of "phase" elements.

References

1. H. C. van de Hulst, Light Scattering by Small Particles Dover, New York, (1957).
2. Huang D., Swanson E. A., Lin C. P., Schuman J. S., Stinson W. G., Chang W., Hee M. R, Flotte T., Gregory K., Puliafito C. A., Fujimoto J. G. Science **254** (1991) 1178.
3. Fercher A.F. J. Biomed. Opt. **1** (1996) 157.
4. Bickel W. S. and Bailey W. M., Am. J. Phys. **53** (1995) 468.
5. J. F. de Boer, Srinivas S. M., Park B. H., Pham T. H., Chen Z., Milner T. E., Nelson J. S. IEEE J..Sel. Top. Quant. Electron. **5** (1999) 1200.
6. J. F. de Boer, Milner T. E., M. J. C. van Gemert, and Nelson J. S. Opt. Lett. **22** (1997) 934.
7. J. F. de Boer, Srinivas S. M., Malekafzali A., Chen Z., and Nelson J. S. Opt. Express **3** (1998) 212.
8. J. F. de Boer, Milner T. E. and Nelson J. S. Opt. Lett. **24** (1999) 300.
9. Yao G. and Wang L.-H. Opt. Lett. **24** (1999) 537.
10. Jiao S.-L., Yao G., and Wang L.-H., Appl. Optics **39** (2000) 6318 .
11. Jiao S. and Wang L.-H. Opt. Lett. **27 (2)** (2002) 101.
12. Jiao S., Yu W., Stoica G. and Wang L.-H. Opt. Lett. **28 (14)** (2003) 1206.
13. Schmitt J. M. and Xiang S. H. Opt. Lett. **23** (1998) 1060.
14. Cowin S.C. J. Biomed. Eng. **122** (2000) 553.
15. Ushenko A.G. Laser Phys. **10 (6)** (2000) 1.
16. Angelsky O.V., Burcovets D.N., Kovalchuk A.V. and Hanson S.T. Appl. Opt. **41(22)** (2002). 4620.
17. Zhao Y.P., Cheng C.F., Wang G.C. and Lu T.M. Surf. Sci. Lett. **409** (1998) L703.
18. Jacques S.L., Alter C.A., Prahl S.A. Lasers Life Sci. **1** (1987) 309.
19. Marchesini R., Bertoni A., Andreola S. et. al. Appl. Opt. **28** (1989) 2318.